ChemSusChem

Research Article
doi.org/10.1002/cssc.202301269

Chemistry Europe
European Chemical Societies Publishing

www.chemsuschem.org

Revealing the Structural Evolution of Electrode/Electrolyte Interphase Formation during Magnesium Plating and Stripping with *operando* EQCM-D

Benjamin W. Schick,[a] Xu Hou,[b] Viktor Vanoppen,[b] Matthias Uhl,[a] Matthias Kruck,[a] Erik J. Berg,[b] and Timo Jacob*[a, c, d]

Rechargeable magnesium batteries could provide future energy storage systems with high energy density. One remaining challenge is the development of electrolytes compatible with the negative Mg electrode, enabling uniform plating and stripping with high Coulombic efficiencies. Often improvements are hindered by a lack of fundamental understanding of processes occurring during cycling, as well as the existence and structure of a formed interphase layer at the electrode/electrolyte interface. Here, a magnesium model electrolyte based on magnesium bis(trifluoromethanesulfonyl)imide ($Mg(TFSI)_2$) and $MgCl_2$ with a borohydride as additive, dissolved in dimethoxyethane (DME), was used to investigate the initial galvanostatic plating and stripping cycles *operando* using electrochemical quartz crystal microbalance with dissipation monitoring (EQCM-D). We show that side reactions lead to the formation of an interphase of irreversibly deposited Mg during the initial cycles. EQCM-D based hydrodynamic spectroscopy reveals the growth of a porous layer during Mg stripping. After the first cycles, the interphase layer is in a dynamic equilibrium between the formation of the layer and its dissolution, resulting in a stable thickness upon further cycling. This study provides *operando* information of the interphase formation, its changes during cycling and the dynamic behavior, helping to rationally develop future electrolytes and electrode/electrolyte interfaces and interphases.

Introduction

Within the field of post-lithium batteries, Mg is a promising candidate for future energy storage due to the low reduction potential, high theoretical volumetric capacity and high abundance.[1,2] To exploit this advantage, metallic Mg is required as a negative electrode. Since the first prototype system about 20 years ago, there were various approaches to find suitable electrolytes and cathodes which can be combined with metallic Mg electrodes.[3–6] However, many challenges have to be overcome for realizing Mg as a negative electrode in a secondary Mg battery. For example, carbonate electrolytes, which are commonly used in lithium ion batteries, cannot be used in combination with metallic Mg due to the formation of a passivation layer which blocks Mg deposition and dissolution.[7] Therefore, it is not possible to transfer the components from lithium ion batteries directly to Mg systems. Furthermore, it was assumed that only small amounts of contaminants, such as H_2O, O_2 or other organic compounds, lead to a reaction with Mg and form a passivating layer where Mg deposition and dissolution is blocked.[7]

Only a limited number of solvents and salts have proven to be compatible with Mg.[7] Ethers, such as tetrahydrofuran, DME or higher glymes, are used as solvents for Mg electrolytes, as they are relatively stable in contact with magnesium.[8] But also in these stable electrolytes, theoretical simulations show that decomposition could occur and compete with Mg deposition.[9,10] Besides other non-nucleophilic salts, $Mg(TFSI)_2$-based electrolytes gained increasing attention within the last years as $Mg(TFSI)_2$ is commercially available and enables Mg deposition. But the overpotentials for Mg stripping are very high and there are signs that the TFSI anion is not stable towards Mg.[11–13] Especially the reduced Mg(I)TFSI shows instabilities and is susceptible to bond cleavage.[12,14,15] The TFSI salt is often used in combination with the chloride salt which leads to higher Coulombic efficiencies and lower overpotentials for plating and stripping.[4,16,17] The exact role of chloride is controversial and still a current topic but it is assumed that chloride changes the composition of Mg-complexes in solution and has an influence on the electrode/electrolyte interface

[a] B. W. Schick, M. Uhl, M. Kruck, Prof. Dr. T. Jacob
Institute of Electrochemistry
Ulm University
Albert-Einstein-Allee 47, 89081 Ulm (Germany)
E-mail: timo.jacob@uni-ulm.de

[b] Dr. X. Hou, V. Vanoppen, Prof. Dr. E. J. Berg
Department of Chemistry – Ångström Laboratory, Structural Chemistry
Uppsala University
Lägerhyddsvägen 1, 752 37 Uppsala (Sweden)

[c] Prof. Dr. T. Jacob
Helmholtz-Institute Ulm (HIU) for Electrochemical Energy Storage
Helmholtzstr. 11, 89081 Ulm (Germany)

[d] Prof. Dr. T. Jacob
Karlsruhe Institute of Technology (KIT)
P.O. Box 3640, 76021 Karlsruhe (Germany)

Supporting information for this article is available on the WWW under https://doi.org/10.1002/cssc.202301269

preventing passivation.[8,18,19] Most of the simple salt electrolytes have a pronounced initial conditioning process during which overpotentials for plating and stripping decrease and Coulombic efficiency increases.[1,20] This process could be connected to the reaction of contaminants in the electrolyte. Borohydrides, such as $Mg(BH_4)_2$ or tetrabutylammonium borohydride ($TBABH_4$), as electrolyte additives, have proven to enable Mg plating and stripping with high Coulombic efficiencies in several electrolyte systems without the need for a conditioning procedure.[21–24]

The already described tendencies to decomposition, which are also present in other electrolyte systems and which lead to Coulombic efficiencies clearly below 100%, raise questions about the whereabouts of possible decomposition products.[20] Until a few years ago, it was assumed that surface films are formed on electrodeposited Mg, leading to unwanted passivation.[7,25] In $Mg(TFSI)_2$ and $MgCl_2$-based electrolytes, formation of porous and nonuniform structures due to partial passivation were reported.[26] In recent years, there have been more and more reports about thin solid electrolyte interphase (SEI) layers which are growing on the Mg electrode surface or on freshly electrodeposited Mg and enable Mg plating and stripping and are even needed for achieving a successfully operating system.[4,12,27] Thus, there are also attempts to create and design the SEI purposefully to improve the electrochemical performance.[4,28,29]

Despite numerous studies of Mg plating/stripping, there are open questions about the formation, composition, and structure of interphases and their influence on the electrochemical behavior. The applied measurement techniques are almost exclusively performed *ex situ*, *e.g.*, by X-ray photoelectron spectroscopy (XPS) or energy dispersive spectroscopy (EDS).[8] These techniques have the disadvantage that changes in structure due to the disassembly of an electrochemical cell, cleaning of the electrode and transfer into the measurement chamber cannot be excluded. Furthermore, they can only measure one fixed state along the battery operation. This means that there is a lack of suitable *operando* investigations on the evolution of interphase layer formation during cycling.[8,12] A better understanding is crucial to rationally design future electrolyte systems leading to higher cycling stability and higher Coulombic efficiencies.[13,18,30]

One *operando* technique which is capable of revealing information about the existence and structural evolution of possibly formed interphases at the electrode/electrolyte interface is the electrochemical quartz crystal microbalance with dissipation monitoring (EQCM-D).[31–35] By recording the resonance frequencies f_n (at multiple overtone orders n) of a metal-coated quartz crystal, which acts as the working electrode at the same time, it is possible to measure mass changes $\triangle m$ of the electrode simultaneously to the electrochemical information. If the surface structure is not flat and the bandwidth is changing during the measurement, more advanced models have to be used to describe the system appropriately (see section 2.1). By also considering the changes in bandwidth $\triangle W_n$ as well as the changes in frequency $\triangle f_n$ for all overtone orders from $n = 3$–13, it is even possible to extract more advanced structural parameters of the surface by applying hydrodynamic spectroscopy for a stiff but non uniform geometry of the surface.[34]

No investigations published so far, to the best of our knowledge, have applied hydrodynamic spectroscopy on Mg deposition and dissolution. For other battery systems, there are measurements published already, which focus on the negative electrode of a battery. For example, EQCM-D investigations on SEI formation in aqueous and non-aqueous Zn-systems as well as on other battery metals, such as Li or Na, are reported.[35] But they merely consider one frequency and bandwidth or only discuss hydrodynamic spectroscopy qualitatively.[36–38]

To investigate interphase formation on the Au-coated quartz crystal electrode, it is necessary to have a high Coulombic efficiency directly from the first cycle. Otherwise, the formed layer would be so thick that the frequency and bandwidth measurement would be inaccurate or even not possible anymore. Therefore, in the present study, a $Mg(TFSI)_2$ and $MgCl_2$-based electrolyte with dimethoxyethane (DME) as solvent and $TBABH_4$ as an additive with a relatively high Coulombic efficiency, low overpotentials and less pronounced conditioning process was chosen as electrolyte to investigate the electrochemical behavior. At the same time, the structural evolution of the working electrode surface during the initial magnesium deposition and dissolution cycles, was monitored *operando* by EQCM-D, applying hydrodynamic spectroscopy. Based on our studies, we uncovered the formation of an interphase layer and its evolution during cycling to get a fundamental understanding. The porous nature of the interphase was revealed as well as its structural changes during Mg plating and stripping. Furthermore, a slow currentless dissolution of the formed interphase layer was observed, indicating that there is a dynamic equilibrium between interphase formation and dissolution.

Results and Discussion

Theoretical Background

In an EQCM experiment, in the simplest case, a rigid and flat deposit on the quartz crystal leads to a decrease in frequency. The change in mass of the electrode can be directly calculated from the change in frequency via the Sauerbrey equation (Equation 1).[39]

$$\Delta f = -\frac{2f_0^2}{A\sqrt{\rho_q \mu_q}}\Delta m \tag{1}$$

Hereby, f_0 is the fundamental frequency of the quartz, A the surface area, ρ_q the density and μ_q the shear modulus of the quartz. This model only applies if the change in bandwidth of the frequency response is zero. However, if more complex surface morphologies are present on the electrode, more advanced models are required to interpret the measurement data. One of these approaches is hydrodynamic spectroscopy, taking into account hydrodynamic interactions between the

oscillation of the coated quartz crystal and the liquid for stiff and non uniform coatings.[40] For this analysis method, odd overtone orders $n = 3–13$ are included along with the corresponding bandwidths $\triangle W_n$.[41,42] $\triangle f_n$ *and* $\triangle W_n$ are plotted *versus* their respective penetration depth δ, which is a function of overtone order, viscosity η_l and density ρ_l of the liquid (Equation 2).

$$\delta = \left(\frac{\eta_l}{\pi n f_0 \rho_l}\right)^{\frac{1}{2}} \tag{2}$$

The hydrodynamic interactions with the liquid result in additional changes in frequency and bandwidth, which is dependent on the respective penetration depth. In the simplest case, if an ideally flat electrode is brought into contact with a liquid, the resulting $\triangle f_n$ values can be calculated by the Kanazawa equation (Equation 3).[34,43–45]

$$\Delta f = -f_0^{\frac{3}{2}} \sqrt{\frac{\eta_l \rho_l}{n\pi \rho_q \mu_q}} \tag{3}$$

By that, it is also possible to describe the relationship between the frequency and bandwidth changes and the penetration depth (Equation 4).[40]

$$\frac{\Delta f + i\Delta W}{n\rho_l f_0^2} = -\frac{\delta}{\left(\mu_q \rho_q\right)^{\frac{1}{2}}} + \frac{i\delta}{\left(\mu_q \rho_q\right)^{\frac{1}{2}}} \tag{4}$$

But there are also models for more complicated morphologies, such as porous structures (Equation S1–S5) and other surface morphologies.[40] These complex functions for $\triangle f_n$ and $\triangle W_n$ were originally developed by Daikhin *et al.*[46,47] By fitting the data to the respective equations, structural information about the surface morphology, such as the height of a porous layer, is accessible and can be extracted.

Electrochemical Measurement

The electrolyte, composed of 115 mM $Mg(TFSI)_2$ and 115 mM $MgCl_2$ in DME with 15 mM $TBABH_4$ as an additive, was used to characterize the electrochemical magnesium deposition and dissolution by EQCM-D. In Figure 1a, the potential profile of 20 galvanostatic plating and stripping cycles with the Au-coated quartz crystal model electrode is shown. Figure 1d shows the magnified view of cycle 10. The potential profile has the typical shape for Mg deposition, starting with an activation step connected with a higher overpotential for the formation of the first nuclei.[27,48] The potential plateau of the plating step is located at about −120 mV *vs.* Mg and the dissolution slightly above 0 V. This demonstrates that the electrolyte enables magnesium plating and stripping with relatively low overpotentials compared to other Mg electrolytes, also represented in the cyclic voltammogram (Figure S1).[12] At the end of dissolution, the potential is rising fast until 1.5 V, indicating that no electrochemical side reactions are occurring in this potential region.

The Coulombic efficiency of all cycles with a current density of 500 $\mu A\,cm^{-2}$, which is calculated from the fraction of stripping charge and deposition charge,[49] is above 90% and increases to a value of about 95% after 10 cycles (Figure 2) under these measurement conditions. Since the Coulombic efficiency is, for a TFSI-based electrolyte, relatively high directly from the first cycle on, the pronounced conditioning process, which is present in borohydride-free electrolytes, was successfully avoided.[16,27] By varying the current density but maintaining the total charge transferred, the Coulombic efficiency increases with increasing current density. This implies that side reactions are happening between electrolyte and Mg. At higher current densities, there is less time for the deposited Mg to react with the electrolyte. For a current density of 1 $mA\,cm^{-2}$, a Coulombic efficiency of about 97% is reached.

Changes in Frequency and Bandwidth

Complementary to the electrochemical measurement, Δf_n and ΔW_n of the quartz crystal were recorded for $n = 3–13$ (Figure 1b/c and Figure S2) with overtone orders 5 and 11 being representative in Figure 1. During the initial Mg deposition step, frequency is decreasing linearly as expected due to the linear relationship between decrease in frequency and increase in mass on the flat electrode, following the Sauerbrey equation (Figure S3a).[39] During dissolution, the frequency is increasing but not returning to the initial value, indicating an incomplete dissolution. In the first cycle, the reversibility in Δf_n is about 72% for overtone order 5 and 79% for overtone order 11. This behavior repeats for the following cycles but the reversibility of Δf_n during deposition and dissolution is increasing from cycle to cycle, leading to a stable value of Δf_{11} of roughly −500 Hz after each stripping step after about 6 cycles. This change in frequency can be interpreted as the formation of an interphase at the gold electrode, consisting of irreversibly electrodeposited magnesium which has at least partially reacted with the electrolyte and therefore passivates. We name this layer of irreversibly deposited Mg "interphase" in this article to differentiate between a beneficial "SEI", known from lithium ion batteries, and the more passivating interphase layer in this case which consists of either reaction products of Mg with the electrolyte or elemental Mg which is housed by a passivation layer. Apparently, the interphase does not have a negative impact on the overpotentials as the potential plateaus for plating and stripping stay stable and the Coulombic efficiency is even increasing. Even though there is an interphase layer remaining on the gold-coated crystal, all the plating steps show the same activation step at the beginning of deposition similar to the bare gold surface. But at the same time, there is also no indication that the formed interphase has a large beneficial impact on the Coulombic efficiency as it is even decreasing within the first two cycles. The interphase mainly consists of Mg and O, revealed by EDS and XPS analysis (Figure S4 and Table S1). But as already mentioned in the introduction, these results must be taken with caution as it is not clear if the oxidation took place already during the measurement or

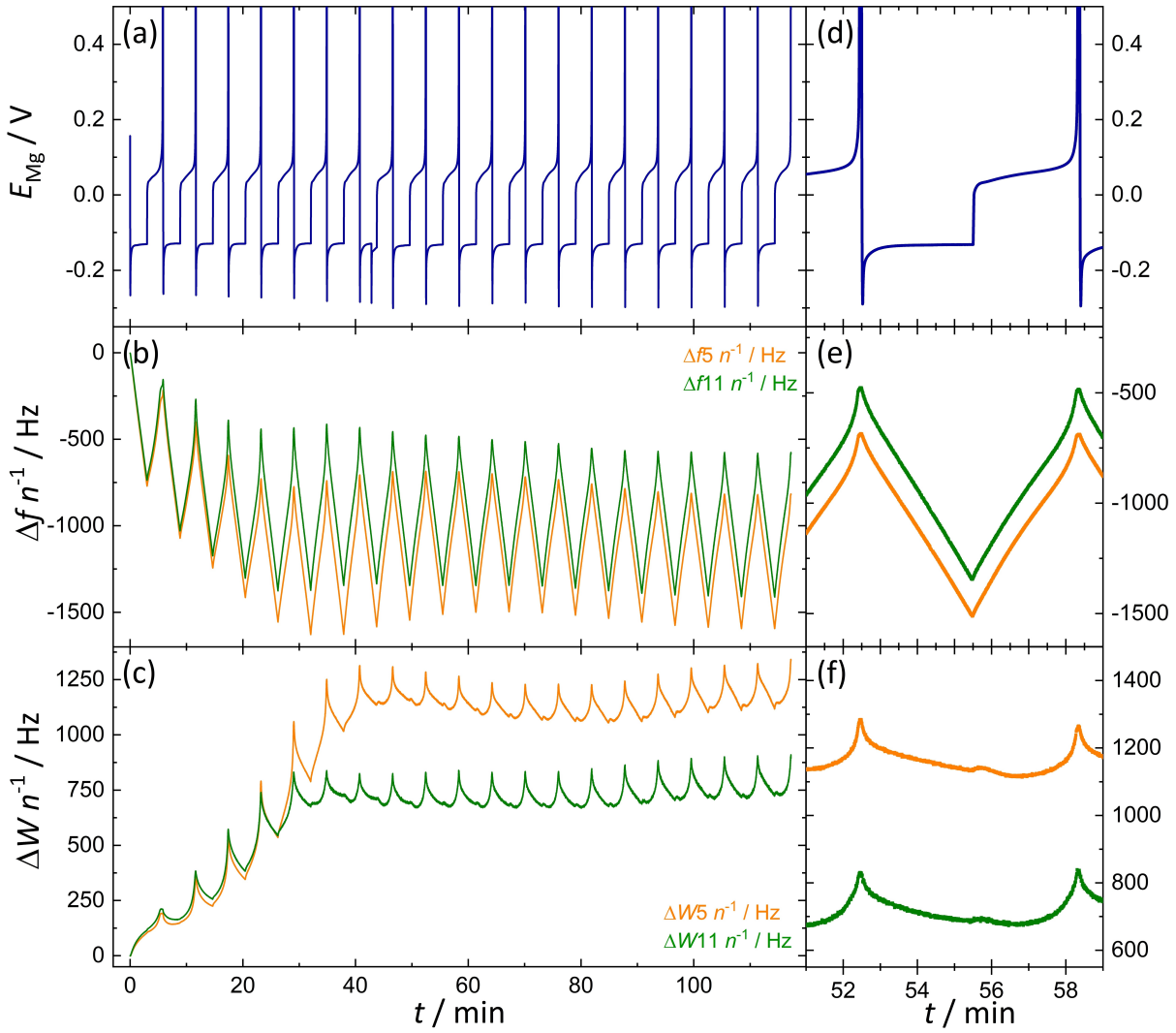

Figure 1. First 20 galvanostatic plating and stripping cycles of the $Mg(TFSI)_2/MgCl_2/TBABH_4$ electrolyte on an Au-coated quartz crystal as working electrode with a current density of 0.5 mA cm^{-2} for 3 min and a cut-off potential of 1.5 V *vs.* Mg for dissolution. (a) potential *vs.* time; (b) change in frequency *vs.* time for the 5th overtone order (orange) and the 11th overtone order (green); (c) change in bandwidth *vs.* time for the 5th overtone order (orange) and the 11th overtone order (green). (d), (e) and (f) show the respective magnified view of cycle 10.

afterwards during disassembly, cleaning, and transfer of the sample. The slope in frequency change during deposition and dissolution is not constant for higher cycle numbers, which cannot be explained by applying the Sauerbrey equation (Figure 1e/f and S3b). The decrease in frequency within the initial cycles is accompanied by an increase in bandwidth before ΔW_n also remains constant from cycle to cycle. For a deposited magnesium layer which is rigid and flat, bandwidth would not change and the change in frequency could be modelled by applying Sauerbrey's equation. Qualitatively, all the overtones behave the same, but the absolute values for Δf_n and ΔW_n are different for the different overtone orders. As the bandwidth is changing strongly and unequal for the different overtone orders, this effect has to be considered. Therefore, hydrodynamic spectroscopy is applied to model Δf_n and ΔW_n of a rigid but more complex coating.[40–42,44] Since the electrodeposition of Mg leads to rigid layers with non uniform geometry, hydrodynamic spectroscopy is applied instead of viscoelastic models which are used for describing soft films on the surface.[34]

Hydrodynamic Spectroscopy

To find a suitable model to express the results for magnesium interphase formation according to its surface morphology, the quartz crystal was analyzed after 20 cycles by scanning electron microscopy (SEM). Figure 3a shows a uniform rough structure on the surface, the more detailed image in Figure 3b reveals a porous structure, with particle sizes not larger than 200 nm. This is also visible in the cross section (Figure 3c) in comparison to the cross section of the bare Au-coated quartz crystal before cycling (Figure S5). The layer is very uniform over the whole surface, making it possible to apply hydrodynamic spectroscopy (Figure S6).

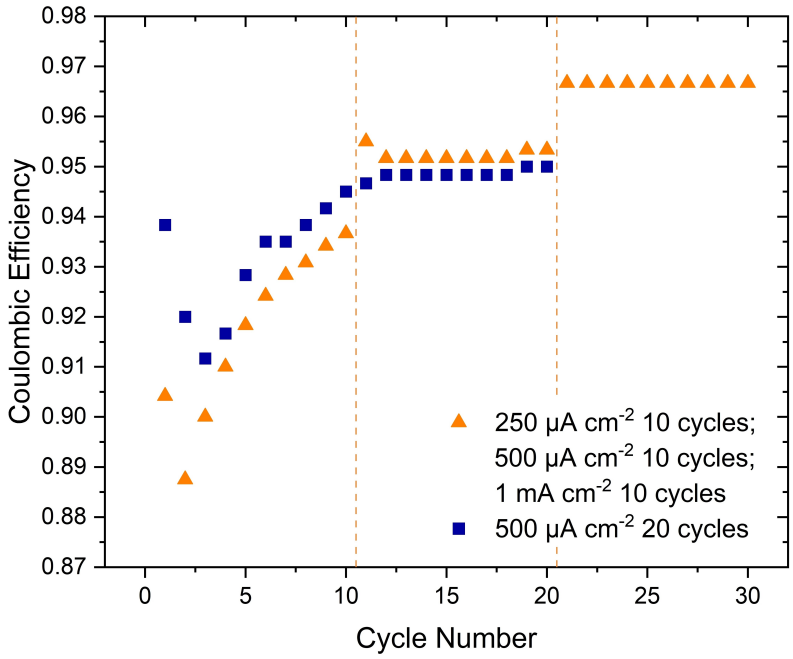

Figure 2. Coulombic efficiency *vs.* time for the first 20 cycles with a current density of 0.5 mA cm^{-2} for a deposition time of 3 min (blue) and for the first 30 cycles with a current density of 0.25 mA cm^{-2} for deposition time of 6 min (cycles 1–10), 0.5 mA cm^{-2} for 3 min (cycles 11–20) and 1 mA cm^{-2} for 90 s (cycles 21–30) (all orange).

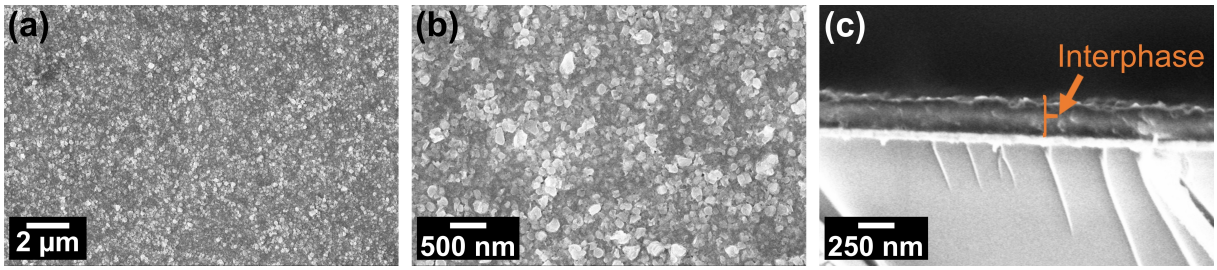

Figure 3. SEM images of the quartz crystal surface after 20 galvanostatic cycles with a scale of 2 µm (a) and a scale of 500 nm (b). Cross section of the quartz crystal after 20 cycles with a scale of 250 nm (c).

Therefore, we chose the model for a uniform porous layer, which Aurbach *et al.* described previously (Equation S1–S5).[33,42] In these equations, the frequency is described by the real part of the complex function and the bandwidth by the imaginary part. By extracting the changes in frequency and bandwidth for all overtones from order 3 to 13, one can receive the corresponding hydrodynamic spectra. Figure 4a–c shows some selected spectra within the first 20 plating and stripping cycles. In these spectra, the positive values on the *y*-axis mark the changes in bandwidth and the negative values are the changes in frequency.[40] The penetration depth (*x*-axis) for the different overtone orders was calculated using an electrolyte density of 0.88 g cm^{-3} and a viscosity of 0.73 mPa s. The lowest overtone has the highest penetration depth, thus, on the contrary, overtone order 13 has the lowest penetration depth. For the spectra of the first cycle (Figure 4a), we selected several specific points in the plating/stripping cycles to show changes in the hydrodynamic spectra.

These points are the initial spectrum before deposition, at half the deposition time, after complete deposition, after half of the dissolution time and at the end of dissolution. The black arrows mark the order of the spectra. The black points in Figure 4a are ascribed to changes in frequency and bandwidth by immersing the bare Au-coated quartz crystal into the electrolyte. In the ideal case for rigid and flat surfaces, the data points are in one line, intersecting with zero at a penetration depth of zero, according to the Kanazawa equation (Equation 3), shown by the black dashed line. The equation was used for the first spectrum before deposition to calculate the viscosity of the electrolyte.[40,43,50]

The bandwidths are increasing for all overtones during deposition which is assigned to the formation of a porous structure. Assuming the complete dissolution of magnesium, one would expect that the bandwidths return to the initial value at the end of dissolution. Contrary to this, the bandwidths further increase during Mg dissolution, which means that a porous structure is remaining on the surface after the first cycle.

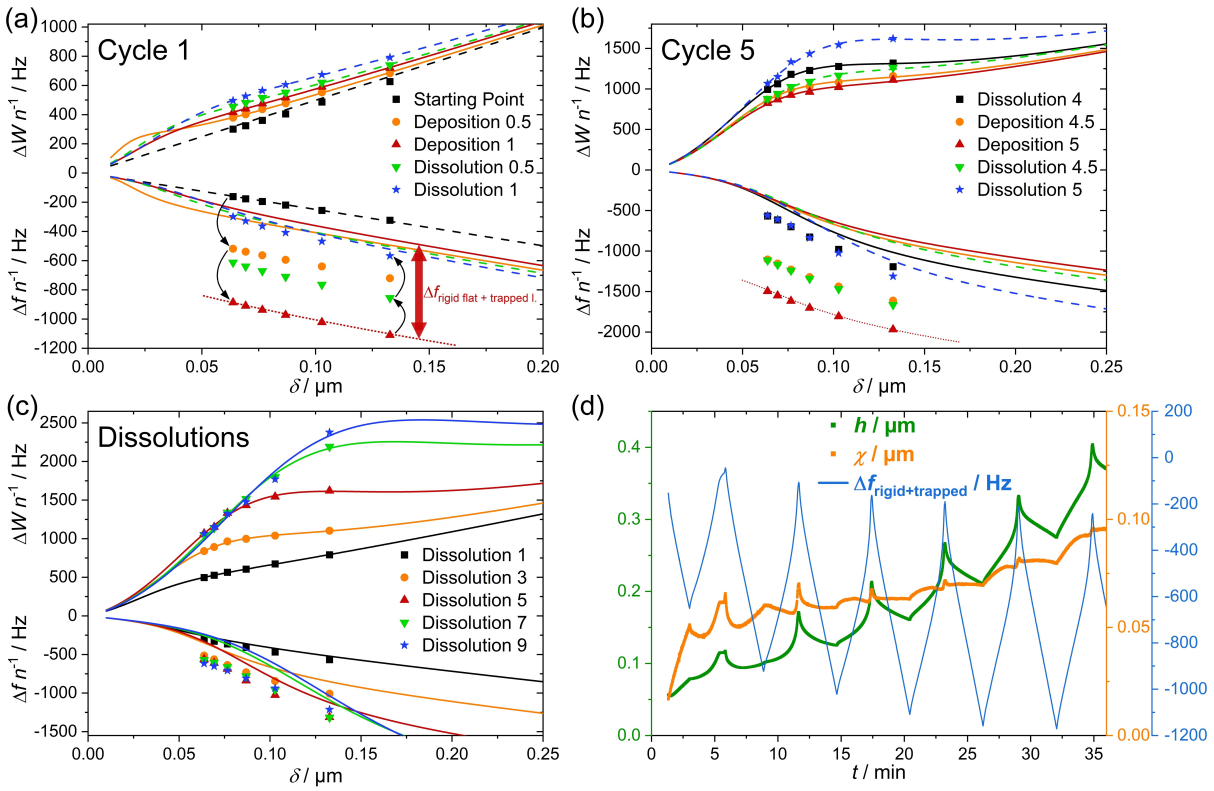

Figure 4. Hydrodynamic spectra of 5 selected points within the first cycle (a) and the fifth cycle (b). Hydrodynamic spectra after the 1st, 3rd, 5th, 7th and 9th cycle (c). Extracted parameters h (green), χ (orange) and $\Delta f_{rigid+trapped}$ (blue) *vs.* time (d).

To further analyze the resulting hydrodynamic spectra and to apply the complex expression for the uniform porous layer, the procedure was the following: First, the data of the changes in bandwidth are considered to fit the function for the uniform porous layer model. Two parameters are extracted from the fit: h is the height of the porous layer and χ is the permeability that correlates with the pore size.[42,44] These extracted parameters are applied to the real part of the complex expression to predict the changes in frequency one would expect from the changes in bandwidth. These are the four lines with a negative slope in Figure 4a. Note, that the fit was not done for the data points before deposition as there is only the flat gold-coated quartz present in the electrolyte, which can be described by Kanazawa's equation but not by a porous layer model. The bare gold-coated quartz crystal without liquid is the reference point for all hydrodynamic spectra. There is a constant offset between the experimental data points and the predicted functions for the frequencies, exemplified by a red double arrow in Figure 4a. Due to the fact that Δf_n and ΔW_n are measured *operando*, there is no reference point of the crystal with deposited Mg in air, like it is demanded in the procedure reported by Shpigel *et al.* This has to be taken into account.[34] As an approximation, it is assumed that the change in bandwidth mainly originates from the hydrodynamic interactions whereas the contribution of the deposit without electrolyte is negligible. The model of the porous layer does not include any rigid flat coating described by the Sauerbrey equation. The plating of Mg leads not only to a porous layer resulting in Δf_n and ΔW_n described by the model of the uniform porous layer, but also to a rigid and flat coating increasing the electrode mass known from the Sauerbrey equation (Equation 1). The latter results in additional Δf_n but not in ΔW_n, leading to the observed constant offset for Δf_n of all overtones. Additionally, liquid which is trapped in narrow pores, smaller than the penetration depth, contributes to the change in frequency without affecting the bandwidth.[51] The formation of porous layers with channels, filled with electrolyte, is also known from other systems such as the alkali metals Li and Na.[52,53] The fact that, despite the offset, the trend of the function fits well to the experimental spectra, shows that the used model is valid. In the ideal case, the differences between the experimental points and the predicted changes in frequency are equidistant for all penetration depths. The red dotted line acts as a guide for the eye, which has the same shape as the predicted curve but with an offset, confirms a reasonable agreement. After complete deposition, the offset between predicted curve and experimental data is largest as this marks the point where the thickness of the deposited Mg layer has its maximum. After dissolution, the frequency is lower than before the cycle for all overtones, which fits to the results of the bandwidth analysis. These findings confirm a report where the formation of a layer after plating and stripping from a $Mg(TFSI)_2$-based electrolyte was described.[27] The report suggested that active Mg is left back which is housed by a passivation layer. This fits to our hydrodynamic spectra as the parts which are passivated are left on the electrode as a porous layer.

To investigate changes during plating and stripping when an interphase is already present on the electrode surface, the hydrodynamic spectra for cycle 5 were also analyzed in detail. The same procedure as for cycle 1 is shown for cycle 5 in Figure 4b. In this case, during deposition, the bandwidth is decreasing in contrast to the first cycle, indicating a shrinking porous layer by filling the pores. The dotted red line as a guide for the eye confirms again that the fit and prediction of the measured frequencies is still reasonable. The stabilization of the interphase thickness after 5 cycles, shown in Figure 1b, is also reflected here. The differences in Δf_n between dissolution 4 and 5 are small compared to the differences between starting point and dissolution 1, which means that the interphase growth slows down. Some selected spectra after a different amount of cycles are shown in Figure 4c, the spectra of the corresponding deposition steps behave similarly and are shown in Figure S7. The evolution of the porous interphase is obvious by the deviation from the straight Kanazawa line recorded before the first deposition. The bandwidths and frequencies for low penetration depths are stabilizing already after about 5 cycles whereas for larger penetration depths, the bandwidths are increasing further. This behavior is not represented in Δf_n as there is almost no change between the measured data points from cycle 5 to 9 for all penetration depths. This divergence is also reflected in the fit. While for cycle 5, the experimental frequencies are still equidistant to the curve predicted from the bandwidths, this is not true for cycle 9 anymore. For low penetration depths, the difference between the predicted curve and the experimental data points for Δf_n is much larger than for high penetration depths, showing that the fit is not accurate. The origin of this could be viscoelastic effects due to loose and inaccessible "dead" magnesium particles which may have been detached from the surface, resulting in higher damping but not in higher mass on the electrode. Another possibility are inhomogeneities which result in an inaccurate fit of the model. Furthermore, the high overtone orders could also deviate as the acoustic wave could probe the viscoelasticity of the porous layer for small penetration depths.[51] After cycle 9, there are almost no changes until cycle 20 (Figure S8). In addition to the selected spectra, the parameters h, χ, and $\Delta f_{\text{rigid}+\text{trapped}}$ which is the contribution of rigid flat coating and liquid trapped in narrow pores, calculated by the average offset between predicted and experimental frequency, of all measurement points were extracted and plotted *vs.* time (Figure 4d).[42] The results for the first 6 cycles are shown as the fit is still accurate in this region. The extracted parameters for the whole 20 cycles are shown in Figure S9. Assuming a completely flat deposition of magnesium in the pure gravimetric case, one would expect a change in frequency of about −640 Hz for deposition, according to the Sauerbrey equation. This fits almost perfectly to the first deposition step (Figure S10a). In the next cycles, the frequency change, attributed to the rigid flat coating, is much larger, approaching −1000 Hz. At the same time the thickness of the porous layer is decreasing during deposition and increasing during dissolution, especially at the beginning and at the end, respectively (Figure S10b). This is also reflected in a higher slope in the frequency change. The hypothesis is that pores are filled upon deposition, which means that they do not contribute to the porous layer anymore but to the rigid flat layer, not resulting in a bandwidth change but in a change in frequency. After the first cycle, the porous layer is already more than 100 nm thick. During dissolution 5, the porous layer is growing by about 100 nm and has a total thickness of about 300 nm after 5 cycles. The further growth of the porous layer is probably an overestimation as the changes in bandwidth for high penetration depths lead to a higher value for h after about 7 cycles where the fit is not accurate anymore. Regardless, the results are in good agreement with the thickness of the interphase measured by SEM. The results are as well consistent with the report of Yoo *et al.*, who described the change from granular nuclei to a porous structure after cycling.[12,26] Compared to this report, where the growth of hemispherical deposits was ascribed to limited sites for Mg deposition, *operando* EQCM-D results give insights into the structural changes and indicate that the porous structure is mainly formed as a result of incomplete Mg dissolution.[26]

Dynamic Behavior of the Interphase

While holding at open circuit potential (*ocp*) for 12 hours after 20 cycles, the changes in frequency and in bandwidth reveal a dynamic behavior (Figure 5a). After the first 20 cycles (Figure 5b), frequency and bandwidth become more stable with increasing cycle number. But when cycling is stopped and the potential is kept at *ocp*, both start to change. While frequency is continuously increasing, bandwidth is decreasing, which means that the formed interphase is dissolving without a net current

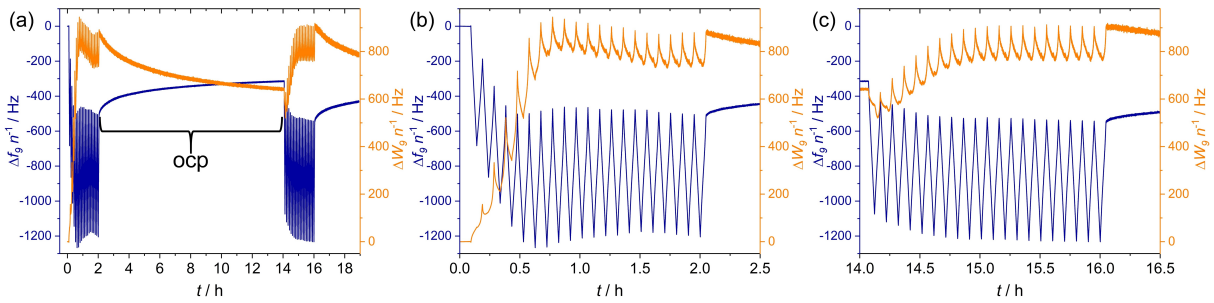

Figure 5. Change in frequency (blue) and in bandwidth (orange) for the 9th overtone order *vs.* time of 40 galvanostatic cycles with 12 hours *ocp* time between the 20th and the 21st cycle (a), magnification of cycle 1–20 (b) and magnification of cycle 21–40.

flow. In the next 20 cycles after staying at *ocp* for 12 hours (Figure 5c), frequency is dropping again whereas bandwidth is increasing from cycle to cycle analogous to the above-described behavior of the fresh and blank electrode. Both, Δf_n and ΔW_n, stabilize again at values that are comparable to those obtained after the first 20 cycles. This leads to the conclusion that the interphase is not stable but in a dynamic equilibrium between its formation and dissolution. This observation can explain why the Coulombic efficiency (Figure 2) does not correlate with the frequency reversibility. The missing 5 percent in Coulombic efficiency compared to the frequency reversibility mainly originate from the reaction of reactive electrolyte parts, most probable TFSI, with deposited magnesium. In another report, the SEI growth at a Mg electrode under open circuit conditions was examined, showing that an interphase is growing in TFSI-based electrolytes, confirming the chemical reaction between the TFSI-based electrolyte and Mg.[54] Further verification would require element specific characterization techniques which are applied *in situ*. As the porous structure is growing during the initial cycles, the surface becomes larger, leading to a higher interphase dissolution rate. The reversibility in frequency after about 6 cycles is at 100% when the interphase is dissolving with the same rate as the interphase is growing during cycling. This means that the dissolution of the interphase and the formation during cycling are in a dynamic equilibrium, leading to the stabilization of interphase thickness. The slight increase in Coulombic efficiency between cycles 3 and 10 could originate from a slower diffusion of reactive electrolyte parts through the porous layer. Slow interphase dissolution does not have a negative impact on the Coulombic efficiency as it is even 0.5% higher in the subsequent cycles (see Figure S11 and 12). Furthermore, an increase in current density, which results in an increase in Coulombic efficiency, leads to a decrease in interphase thickness (see Figure S13 and 14). A new dynamic equilibrium is established, which is reflected in the different frequency and bandwidth plateaus for the three current densities. The slow, currentless dissolution can also explain the appearance of dead Mg particles which are detaching from the surface. The slow dissolution could be related to the passivation layer, building a new, bare Mg surface of previously housed Mg, which reacts with the electrolyte. This results in a new passivation layer which again dissolves.

Layer Removal at High Potentials

The interphase is not only dissolving while staying at *ocp*, but can also be more rapidly removed at high potentials (Figure 6). After 10 plating and stripping cycles, a potential of 2.5 V *vs.* Mg was applied for 90 s. The frequency as well as the bandwidth return to the original values for the bare Au-coated quartz crystal within one minute. The removal of the interphase layer is accompanied by hydrogen evolution, investigated by online electrochemical mass spectrometry (Figure S15). H_2 evolution is most probably caused by borohydride decomposition.[21,22] Besides this, no gas formation was detected, which means that no typical decomposition gases such as H_2 or CO_2 are forming

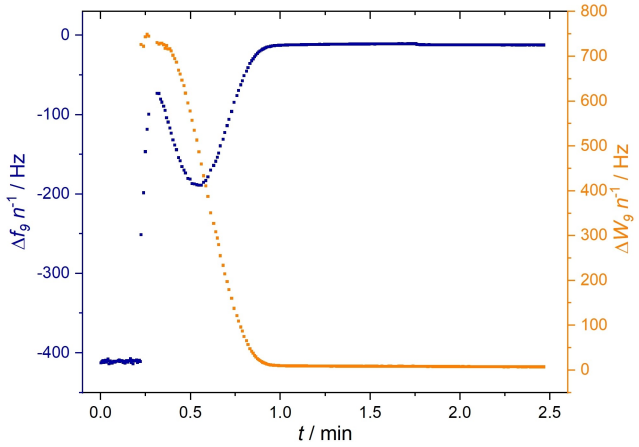

Figure 6. Chronoamperometric measurement at 2.5 V *vs.* Mg for 90 s. Change in frequency (blue) and in bandwidth (orange) for the 9th overtone order *vs.* time.

during Mg plating and stripping. The mechanism of this layer removal remains unclear. One possibility is spalling of the interphase caused by the gas formation at the electrode surface. Another explanation is the removal of the thin passivation layer, which houses the active magnesium, by the reactive hydrogen. By removing the thin passivation layer, the magnesium can be electrochemically stripped (Figure S16). It is also possible that the borohydride decomposition is not involved in the layer removal. Holc *et al.* reported about an interphase oxidation, too.[27] But in their case, the TFSI-based electrolyte didn't contain any borohydride but a similar effect was still observed at high potentials.

The frequency profile as well as the potential profile are almost identical in the ten cycles before and after layer removal (Figure S17 and S18). One interesting observation, which further supports the hypothesis of dead magnesium particles forming during cycling, is the layer removal after 20 cycles (Figure S19). In this case the frequency, especially for high overtones, returns to its initial values. This is not the case for the bandwidth as especially the overtones with a high penetration depth do not reach the initial values, which means that particles remain on the surface which lead to a higher dissipation.

Implications for the Structural Evolution of the Interphase

In Figure 7, the results from Figure 1–6 are visualized. They are in good agreement with the results proposed by Sun *et al.* but with additional information on the dynamic behavior and the changes during plating and stripping.[12] The dark grey part marks the deposited magnesium and the formed interphase which contributes to the rigid flat coating, resulting in a change in frequency but not in bandwidth. The bright grey part represents the porous structure which results in a change in bandwidth. In the first deposition step, magnesium is not deposited as a completely flat coating. During dissolution, the layer height of the porous interphase is increasing, especially at the end of dissolution. In the next plating steps, the thickness

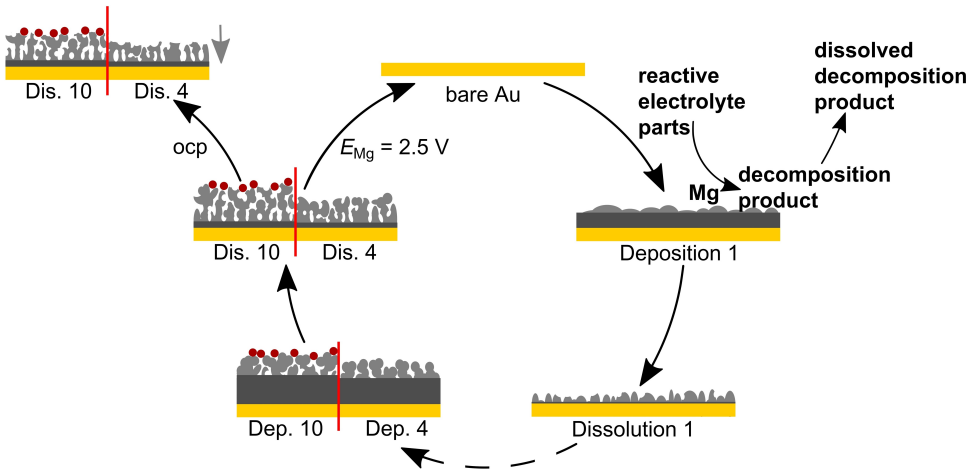

Figure 7. Visualization of interphase formation obtained from EQCM-D results. The bright grey part is the porous layer, dark grey marks the $\Delta f_{rigid+trapped}$, which is described by the Sauerbrey equation, and red the dead Mg particles which have detached from the surface.

of the porous layer is decreasing during deposition as the pores are filled up by magnesium, whereas the porous layer is getting thicker during dissolution as pores are formed due to incomplete dissolution. By that, a porous interphase is evolving during the first cycles. The formed interphase does apparently not lead to passivation of the electrode but behaves as the noble electrode substrate at the beginning. The interphase shows a dynamic behavior as it is slowly dissolving at *ocp*. The thickness of the interphase is stabilizing during operation after about 6 cycles as a dynamic equilibrium between interphase formation and dissolution is reached. At high potentials, the layer is removed, accompanied by hydrogen evolution, and is forming again in the subsequent cycles.

Conclusions

In summary, using electrochemical quartz crystal microbalance with dissipation monitoring (EQCM-D) the initial galvanostatic plating and stripping cycles from a magnesium model electrolyte was studied under operation conditions. We found that reversible magnesium plating and stripping with a high Coulombic efficiency is possible with the investigated electrolyte, based on $Mg(TFSI)_2$, $MgCl_2$ and $TBABH_4$ in DME. But side reactions, lowering the Coulombic efficiency, are occurring also in this electrolyte, which lead to passivated magnesium remaining at the electrode, forming porous structures. Structural changes during cycling are dominated by a growth of the porous layer during dissolution and a shrinking during deposition due to a consecutive emptying and filling of the pores. It is important to consider these formed layers as they have an influence on the structure of magnesium deposition and dissolution even after the layer has stopped growing. Furthermore, the unexpected dynamic behavior due to the slow dissolution of the interphase was revealed, which leads to a dynamic equilibrium between interphase formation and dissolution during cycling. Transferred to a magnesium metal electrode, this means that a porous interphase is forming during cycling and the electrode is slowly degrading in this electrolyte. Future investigations which comprise element specific characterization techniques, in the best case under operating conditions, would be highly interesting to get deeper insights into the observed phenomena. Understanding the processes and collecting information about the existence and structural evolution of interphases will help to rationally design new types of electrolytes and actively tune the interface and interphase between electrode and electrolyte. Therefore, our work can help adjusting the cycling parameters during conditioning to find an optimum for the reversible magnesium deposition for the negative electrode of a magnesium metal battery. *Operando* characterization of magnesium deposition and dissolution was successfully demonstrated, applying hydrodynamic spectroscopy to analyse changes in frequency and bandwidth, including the overtone orders up to the 13^{th} overtone. The presented methodology opens up for a more targeted and effective design approach to identify and optimize the role of each electrolyte component, e.g. layer-forming additive, towards high-performance interphases for Mg batteries and other energy storage systems.

Experimental Section

The electrolyte was prepared by mixing 115 mM $Mg(TFSI)_2$ (99.5%, Solvionic), 115 mM $MgCl_2$ (99.9%, Alfa Aesar) and 15 mM $TBABH_4$ (98%, Sigma-Aldrich) with DME (99.5%, Sigma-Aldrich). The electrolyte was handled under inert atmosphere (O_2 <0.5 ppm, H_2O <0.5 ppm). $Mg(TFSI)_2$ was dried at 80 °C for 24 hours and 10^{-3} mbar prior to use. $MgCl_2$ and $TBABH_4$ were used as received. DME was dried over molecular sieve for several days prior to use, resulting in a water content below 10 ppm, tested by Karl Fischer Titration (KF-Coulometer 851 by Metrohm, with Hydranal Coulmat AG electrolyte by Honeywell). After mixing, the electrolyte was stirred for several hours at 50 °C.

EQCM-D measurements were done with a Q-Sense system from Biolin Scientific, Sweden. The measurement cell was custom-made. The closed cell was assembled in a glove box and transferred to the measurement device, which was positioned in a box with constant

nitrogen flow. Mg plate (99.9%, Goodfellow) with a diameter of 12 mm served as counter electrode and Mg wire (99.9%, Goodfellow) as the reference electrode. Both were cleaned with sand paper under inert conditions prior to use. As working electrode, an Au-coated 5 MHz quartz crystal (Biolin Scientific) was used. Between counter and reference electrode, there was a glass fibre separator with a diameter of 13 mm (Whatman, GF/A). An electrolyte volume of 0.4 mL was required for one measurement. The electrochemical measurement in parallel to the QCM measurement was done with a PalmSense MultiEmStat4 HR (Palmsens B.V.). All measurements were performed at room temperature. Magnesium was first deposited galvanostatically with a current density of $-500\ \mu A\,cm^{-2}$ for 3 minutes, followed by magnesium dissolution at $500\ \mu A\,cm^{-2}$ until the potential reached a value of 1.5 V *vs.* Mg. This was the typical procedure if not described differently.

SEM images were recorded with a Zeiss LEO 1550 Microscope, using the in-lens secondary electron detectors. Images were acquired at 5.0 kV acceleration voltage. After the measurement, the cell was disassembled and transferred to the device without further cleaning. A spot without residual electrolyte was selected for the measurement.

Au-mesh electrodes for the OEMS measurements were prepared by sputtering Au on both sides of a stainless steel mesh (212/90 μm, Bopp AG, Switzerland) and the punch to correct size (ø 15 mm). To increase the electrochemical surface area of the Au-mesh electrodes, two mesh electrodes were stacked on top of each other. The electrochemical cells and the data treatment procedure for operando measurements has been described in previous publications. All measurements were performed at 30 °C.

Supporting Information

Supporting Information is available from the Wiley Online Library or from the author.

Acknowledgements

We thank Dr. Joachim Bansmann for XPS measurements and Dr. Mohammad Al-Shakran for SEM/EDS measurements. We also thank Dr. Maximilian U. Ceblin, Dr. Attila Farkas and Tanja Geng for fruitful discussions. We thank the German Research Foundation (DFG) for funding under Project ID 390874152 (POLiS Cluster of Excellence), as well as for funding within the priority program SPP 2248 Polymer-based Batteries (Project ID 441209207) and through the individual project with ID 501805371. X.H., V.V., and E.J.B acknowledge Knut and Alice Wallenberg (KAW) Foundation (Grant 2017.0204), Stiftelsen för Strategisk Forskning (SSF, FFL18- 0269)), and StandUp for Energy for financial support. Open Access funding enabled and organized by Projekt DEAL.

Conflict of Interests

The authors declare no conflict of interest.

Data Availability Statement

The data that support the findings of this study are available from the corresponding author upon reasonable request.

Keywords: magnesium battery · EQCM-D · electrochemistry · interphase · electrolyte · hydrodynamic spectroscopy · structure

[1] I. Shterenberg, M. Salama, Y. Gofer, E. Levi, D. Aurbach, *MRS Bull.* **2014**, *39*, 453–460.
[2] J. Muldoon, C. B. Bucur, T. Gregory, *Chem. Rev.* **2014**, *114*, 11683–11720.
[3] D. Aurbach, Z. Lu, A. Schechter, Y. Gofer, H. Gizbar, R. Turgeman, Y. Cohen, M. Moshkovich, E. Levi, *Nature* **2000**, *407*, 724–727.
[4] Z. Liang, C. Ban, *Angew. Chem. Int. Ed.* **2021**, *60*, 11036–11047.
[5] R. Dominko, J. Bitenc, R. Berthelot, M. Gauthier, G. Pagot, V. Di Noto, *J. Power Sources* **2020**, *478*, 229027.
[6] F. Liu, T. Wang, X. Liu, L. Z. Fan, *Adv. Energy Mater.* **2021**, *11*, 2000787.
[7] R. Attias, M. Salama, B. Hirsch, Y. Goffer, D. Aurbach, *Joule* **2019**, *3*, 27–52.
[8] J. D. Forero-Saboya, D. S. Tchitchekova, P. Johansson, M. R. Palacín, A. Ponrouch, *Adv. Mater. Interfaces* **2022**, *9*, 2101578.
[9] T. J. Seguin, N. T. Hahn, K. R. Zavadil, K. A. Persson, *Front. Chem.* **2019**, *7*, 175.
[10] A. Kopač Lautar, J. Bitenc, T. Rejec, R. Dominko, J. S. Filhol, M. L. Doublet, *J. Am. Chem. Soc.* **2020**, *142*, 5146–5153.
[11] N. Sa, N. N. Rajput, H. Wang, B. Key, M. Ferrandon, V. Srinivasan, K. A. Persson, A. K. Burrell, J. T. Vaughey, *RSC Adv.* **2016**, *6*, 113663–113670.
[12] Y. Sun, F. Ai, Y. C. Lu, *Small* **2022**, *18*, 2200009.
[13] W. Zhao, Y. Liu, X. Zhao, Z. Pan, J. Chen, S. Zheng, L. Qu, X. Yang, *Chem. Eur. J.* **2023**, *29*, e202203334.
[14] N. N. Rajput, X. Qu, N. Sa, A. K. Burrell, K. A. Persson, *J. Am. Chem. Soc.* **2015**, *137*, 3411–3420.
[15] A. Baskin, D. Prendergast, *J. Phys. Chem. C* **2016**, *120*, 3583–3594.
[16] I. Shterenberg, M. Salama, H. D. Yoo, Y. Gofer, J.-B. Park, Y.-K. Sun, D. Aurbach, *J. Electrochem. Soc.* **2015**, *162*, A7118–A7128.
[17] N. Sa, B. Pan, A. Saha-Shah, A. A. Hubaud, J. T. Vaughey, L. A. Baker, C. Liao, A. K. Burrell, *ACS Appl. Mater. Interfaces* **2016**, *8*, 16002–16008.
[18] J. G. Connell, B. Genorio, P. P. Lopes, D. Strmcnik, V. R. Stamenkovic, N. M. Markovic, *Chem. Mater.* **2016**, *28*, 8268–8277.
[19] M. Salama, I. Shterenberg, L. J. W. Shimon, K. Keinan-Adamsky, M. Afri, Y. Gofer, D. Aurbach, *J. Phys. Chem. C* **2017**, *121*, 24909–24918.
[20] R. Attias, B. Dlugatch, O. Blumen, K. Shwartsman, M. Salama, N. Shpigel, D. Sharon, *ACS Appl. Mater. Interfaces* **2022**, *14*, 30952–30961.
[21] R. Horia, D. T. Nguyen, A. Y. S. Eng, Z. W. Seh, *Nano Lett.* **2021**, *21*, 8220–8228.
[22] Z. Li, T. Diemant, Z. Meng, Y. Xiu, A. Reupert, L. Wang, M. Fichtner, Z. Zhao-Karger, *ACS Appl. Mater. Interfaces* **2021**, *13*, 33123–33132.
[23] H. Wang, X. Feng, Y. Chen, Y. S. Liu, K. S. Han, M. Zhou, M. H. Engelhard, V. Murugesan, R. S. Assary, T. L. Liu, W. Henderson, Z. Nie, M. Gu, J. Xiao, C. Wang, K. Persson, D. Mei, J. G. Zhang, K. T. Mueller, J. Guo, K. Zavadil, Y. Shao, J. Liu, *ACS Energy Lett.* **2020**, *5*, 200–206.
[24] Z. Ma, M. Kar, C. Xiao, M. Forsyth, D. R. MacFarlane, *Electrochem. Commun.* **2017**, *78*, 29–32.
[25] R. Deivanayagam, B. J. Ingram, R. Shahbazian-Yassar, *Energy Storage Mater.* **2019**, *21*, 136–153.
[26] H. D. Yoo, S. D. Han, I. L. Bolotin, G. M. Nolis, R. D. Bayliss, A. K. Burrell, J. T. Vaughey, J. Cabana, *Langmuir* **2017**, *33*, 9398–9406.
[27] C. Holc, K. Dimogiannis, E. Hopkinson, L. R. Johnson, *ACS Appl. Mater. Interfaces* **2021**, *13*, 29708–29713.
[28] H. Dou, X. Zhao, Y. Zhang, W. Zhao, Y. Yan, Z. F. Ma, X. Wang, X. Yang, *Nano Energy* **2021**, *86*, 106087.
[29] Y. Li, P. Zuo, R. Li, H. Huo, Y. Ma, C. Du, Y. Gao, G. Yin, R. S. Weatherup, *ACS Appl. Mater. Interfaces* **2021**, *13*, 24565–24574.
[30] J. Zhang, Z. Chang, Z. Zhang, A. Du, S. Dong, Z. Li, G. Li, G. Cui, *ACS Nano* **2021**, *15*, 15594–15624.
[31] Z. Yang, M. C. Dixon, R. A. Erck, L. Trahey, *ACS Appl. Mater. Interfaces* **2015**, *7*, 26585–26594.
[32] A. A. Hubaud, Z. Z. Yang, D. J. Schroeder, F. Dogan, L. Trahey, J. T. Vaughey, *J. Power Sources* **2015**, *282*, 639–644.
[33] V. Dargel, N. Shpigel, S. Sigalov, P. Nayak, M. D. Levi, L. Daikhin, D. Aurbach, *Nat. Commun.* **2017**, *8*, 1389.

[34] N. Shpigel, M. D. Levi, S. Sigalov, L. Daikhin, D. Aurbach, *Acc. Chem. Res.* **2018**, *51*, 69–79.
[35] Y. Ji, Z.-W. Yin, Z. Yang, Y.-P. Deng, H. Chen, C. Lin, L. Yang, K. Yang, M. Zhang, Q. Xiao, J.-T. Li, Z. Chen, S.-G. Sun, F. Pan, *Chem. Soc. Rev.* **2021**, *50*, 10743–10763.
[36] L. Seidl, N. Bucher, E. Chu, S. Hartung, S. Martens, O. Schneider, U. Stimming, *Energy Environ. Sci.* **2017**, *10*, 1631–1642.
[37] S. Cora, S. Ahmad, N. Sa, *ACS Appl. Mater. Interfaces* **2021**, *13*, 10131–10140.
[38] K. S. Smaran, S. Shibata, A. Omachi, A. Ohama, E. Tomizawa, T. Kondo, *J. Phys. Chem. Lett.* **2017**, *8*, 5203–5208.
[39] G. Sauerbrey, *Z. Phys.* **1959**, *155*, 206–222.
[40] M. D. Levi, N. Shpigel, S. Sigalov, V. Dargel, L. Daikhin, D. Aurbach, *Electrochim. Acta* **2017**, *232*, 271–284.
[41] N. Shpigel, M. D. Levi, D. Aurbach, *Energy Storage Mater.* **2019**, *21*, 399–413.
[42] S. Sigalov, N. Shpigel, M. D. Levi, M. Feldberg, L. Daikhin, D. Aurbach, *Anal. Chem.* **2016**, *88*, 10151–10157.
[43] K. K. Kanazawa, *Anal. Chem.* **1985**, *57*, 1771–1772.
[44] N. Shpigel, M. D. Levi, S. Sigalov, O. Girshevitz, D. Aurbach, L. Daikhin, P. Pikma, M. Marandi, A. Jänes, E. Lust, N. Jäckel, V. Presser, *Nat. Mater.* **2016**, *15*, 570–575.
[45] K. Keiji Kanazawa, J. G. Gordon II, *Anal. Chim. Acta* **1985**, *175*, 99–105.
[46] L. Daikhin, M. Urbakh, *Langmuir* **1996**, *12*, 6354–6360.
[47] L. Daikhin, E. Gileadi, G. Katz, V. Tsionsky, M. Urbakh, D. Zagidulin, *Anal. Chem.* **2002**, *74*, 554–561.
[48] J. Eaves-Rathert, K. Moyer, M. Zohair, C. L. Pint, *Joule* **2020**, *4*, 1324–1336.
[49] J. Xiao, Q. Li, Y. Bi, M. Cai, B. Dunn, T. Glossmann, J. Liu, T. Osaka, R. Sugiura, B. Wu, J. Yang, J. G. Zhang, M. S. Whittingham, *Nat. Energy* **2020**, *5*, 561–568.
[50] M. D. Levi, L. Daikhin, D. Aurbach, V. Presser, *Electrochem. Commun.* **2016**, *67*, 16–21.
[51] N. Shpigel, S. Sigalov, F. Malchik, M. D. Levi, O. Girshevitz, R. L. Khalfin, D. Aurbach, *Nat. Commun.* **2019**, *10*, 4394.
[52] K. Lim, B. Fenk, J. Popovic, J. Maier, *ACS Appl. Mater. Interfaces* **2021**, *13*, 51767–51774.
[53] K. Lim, J. Popovic, J. Maier, *J. Mater. Chem. A* **2023**, *11*, 5725–5733.
[54] J. Popovic, *Energy Technol.* **2021**, *9*, 2001056.

Manuscript received: September 19, 2023
Revised manuscript received: October 17, 2023
Accepted manuscript online: October 17, 2023
Version of record online: ■■, ■■

RESEARCH ARTICLE

Understanding the formation of interphases at the electrode/electrolyte interface is crucial to rationally develop improved electrolytes for rechargeable magnesium batteries. *Operando* electrochemical quartz crystal microbalance with dissipation monitoring is used to investigate interphase formation during magnesium plating and stripping. The evolution of a porous structure and a dynamic equilibrium between interphase formation and dissolution are revealed.

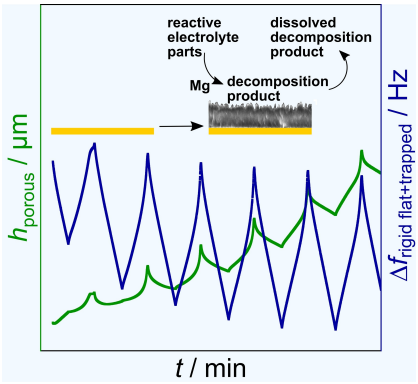

*B. W. Schick, Dr. X. Hou, V. Vanoppen, M. Uhl, M. Kruck, Prof. Dr. E. J. Berg, Prof. Dr. T. Jacob**

1 – 12

Revealing the Structural Evolution of Electrode/Electrolyte Interphase Formation during Magnesium Plating and Stripping with *operando* EQCM-D